Available online at www.sciencedirect.com
SCIENCE DIRECT®
Computers and Geotechnics 32 (2005) 411–421
COMPUTERS AND GEOTECHNICS
www.elsevier.com/locate/compgeo

Lateral performance of piles evaluated via inclinometer data

San-Shyan Lin [a,*], Jen-Cheng Liao [a], J.T. Chen [a], Li Chen [b]

[a] Department of Harbour and River Engineering, National Taiwan Ocean University, Keelung, Taiwan, 20224, Taiwan
[b] Shu Zen College of Medicine and Management, No. 452, Hwan-Chiou Road, Kaohsiung County, Taiwan 821, Taiwan

Received 10 January 2005; received in revised form 30 May 2005; accepted 20 July 2005
Available online 19 September 2005

Abstract

The performance of laterally loaded piles is often obtained via in situ lateral pile–load tests. In general, inclinometer measurement is routinely used in these lateral pile–load tests. In an effort to develop an efficient method for interpretation of lateral pile–load test results via measured inclinometer data only, an analytical model is proposed based on the energy conservation of the pile–soil system. A Fourier series function is used to represent the deflection behaviour of the pile–soil system. To obtain the shear, moment and soil reaction along the pile shaft, convergence of the series after differentiation is guaranteed by applying the Cesaro sum technique. Three full-scale lateral pile–load cases are then used to verify the feasibility of the methodology developed, as well as to make comparisons with other methods.

Keywords: Lateral pile–load test; Inclinometer; *p–y* Curve; Cesaro sum technique

1. Introduction

Inclinometer measurements are routinely used in lateral pile–load tests. If more detailed information such as a *p–y* curve is required, a large number of strain gauges are installed along the length of the pile shaft to develop the bending moment versus depth relationship [1]. The use of slope inclinometers to measure lateral deflection of the pile has some advantages compared to strain gauges, which are easily damaged during pile installation or by improper handling. One further advantage of inclinometer measurement is its low cost. However, a disadvantage of the inclinometer is the level of data reduction errors, because the slope must be differentiated three times to obtain *p–y* curves [1,2].

Brown et al. [2] proposed a method for interpreting the lateral load test. The method utilised a least-square regression technique that will converge to a solution for the analytical *p–y* curves that produces minimum error between the predicted and measured deflection versus depth profile over a range of loading. However, the predicted deflection obtained via another finite-difference computer code, COM624 [3], is required. In addition, assumption of the shape of the curve and iteration over two or more soil parameters are needed to calibrate the *p–y* curves. A method that requires iteration of a single parameter, i.e., the modulus of lateral soil reaction, was proposed by Pinto et al. [1]. However, the initial slope of the *p–y* curves was assumed to increase linearly with depth, which in general can only be used for uniform sands.

In an effort to develop a simple yet accurate method for interpreting lateral load test results for a single pile or a pile group based only on measured inclinometer data, a new method is proposed in this paper. The pile–soil interaction response is idealised as a beam in a Winkler spring medium. A Fourier series function is used as the deflection function of the pile–soil system. Application of the Fourier series in

* Corresponding author. Tel.: +886 2 24622192x6139; fax: +886 2 24623679.
E-mail address: sslin@mail.ntou.edu.tw (S.-S. Lin).

0266-352X/$ - see front matter © 2005 Elsevier Ltd. All rights reserved.
doi:10.1016/j.compgeo.2005.07.003

structural mechanics problems, such as buckling or vibration analysis of beams or plates, has been proved by Chen et al. [4] and Wang and Lin [5]. To derive the slope, shear, moment and soil reaction of the pile, convergence of the series after differentiation is guaranteed by applying the Cesaro sum technique [6]. In this paper, we first present the theory and analytical model development of the proposed method. Three full-scale lateral pile load cases are then used to verify the feasibility of the methodology developed and to make comparisons with other methods.

2. Theory

In the following, the deflection function of lateral loaded piles was derived on the basis of energy conservation concepts, with the calculus of variation. Measured inclinometer data from a lateral loading pile test, which implicitly includes the pile–soil–pile interaction and soil response effect, were used to determine the coefficients of the derived deflection function. Once the deflection function is established, the bending moment, shear force, and p–y reaction at various depths along the pile can be deduced by differentiating the deflection function. Assumptions in the derivation include:

1. Soil deposits are idealised as a non-linear spring system.
2. Pile material is assumed to follow linear elastic behaviour.
3. Lateral loading is applied only at the free pile head for single piles or at the ground surface where the pile cap is located for capped pile groups.

2.1. Energy method

The total energy for a pile embedded in the soil medium is given as

$$\Pi = U + V, \tag{1}$$

where U is strain energy stored in the soil–pile system, and V is the potential energy of the soil–pile system caused by external loads.

As shown in Fig. 1, the strain energy of the soil–pile system can be expressed as

$$U = \frac{1}{2}\int_0^L EI(y'')^2\,\mathrm{d}z, \tag{2}$$

where E is the elastic modulus of the pile, I is the moment of inertia of the pile, y is lateral deflection of the pile, y'' is the second derivative of y, and z is depth along the pile shaft.

The potential energy of the soil–pile system caused by external loading can be expressed as

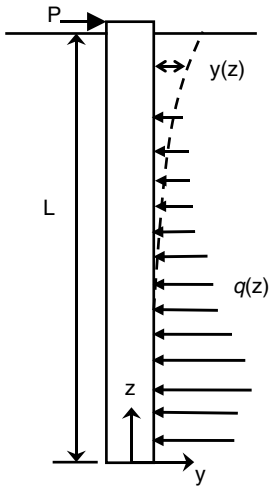

Fig. 1. Schematic diagram of soil–pile system.

$$V = \frac{1}{2}\int_0^L q(z)y\,\mathrm{d}z - Py(L), \tag{3}$$

where $q(z)$ is the soil reaction at depth z, P is lateral force applied at the pile head, $y(L)$ is pile deflection at the pile head, and L is the embedded length of the pile.

Substituting Eqs. (2) and (3) into Eq. (1), the total potential energy of the soil–pile system can be expressed as

$$\Pi = \frac{1}{2}\int_0^L EI(y'')^2\,\mathrm{d}z + \frac{1}{2}\int_0^L q(z)y\,\mathrm{d}z - Py(L). \tag{4}$$

Subsequently, by applying the calculus of variation [7] to Eq. (4), the following Euler–Lagrangian governing equation for the pile–soil system can be obtained [7]:

$$EIy^{\mathrm{IV}} + q(z) = 0. \tag{5}$$

2.2. Deflection functions

Two different boundary conditions for long piles are considered, as shown in Fig. 2. The first case (Case I) considers a free head and fixed toe condition, which represents long piles without caps (Fig. 2(a)). The second case (Case II) considers a fixed head with sway and a fixed toe condition, which represents long piles constrained with caps at the pile head.

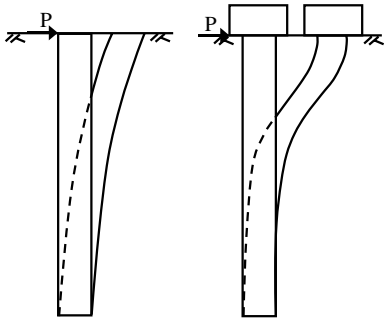

Fig. 2. Boundary conditions of considered in the paper.

By applying the Rayleigh–Ritz method, the general form of deflection functions that satisfies Eq. (5) can then be determined by the following Fourier series:

$$y(z) = \sum_{n=1}^{k} B_n(1 - \cos \bar{N}\pi z), \tag{6}$$

where $\bar{N} = 2n - 1/2L$ and $\bar{N} = n/L$ represent the boundary conditions of Case I and Case II, respectively. The deflection function given in Eq. (6) is used to approximate the pile deflection along the shaft obtained from the measured inclinometer data.

Coefficients B_n can be determined by substituting Eq. (6) into Eq. (4) and by applying minimum potential theory ($\frac{\partial \Pi}{\partial B_n} - 0$), for the Case I boundary conditions, to give

$$EIB_n\left(\frac{2n-1}{2L}\pi\right)^4 \times \frac{1}{2}L + \frac{1}{2}EI\left\{-2B_n\left(\frac{2n-1}{2L}\right)^3 \times \sin\left(\frac{2n-1}{2}\pi\right) + 2B_n\left(\frac{2n-1}{2L}\pi\right)^4 \times \frac{1}{2}L - \sum_{n,m=1}^{k} B_m\left(\frac{2n-1}{2L}\right)^3 \sin\left(\frac{2n-1}{2}\pi\right)\right\} = P, \tag{7}$$

in which $n,m = 1,\ldots,k$. Eq. (7) can also be expressed in the following matrix form:

$$\begin{bmatrix} D_{11} & \cdots & D_{1(n-1)} & D_{1n} \\ D_{21} & \cdots & D_{2(n-1)} & D_{2n} \\ \vdots & \cdots & \vdots & \vdots \\ D_{m1} & \cdots & D_{m(n-1)} & D_{mn} \end{bmatrix}_{m\times n} \begin{Bmatrix} B_1 \\ \vdots \\ B_{n-1} \\ B_n \end{Bmatrix}_{n\times 1} = \begin{Bmatrix} P_1 \\ \vdots \\ P_{m-1} \\ P_m \end{Bmatrix}_{m\times 1}, \tag{8}$$

where

$$D_{mn} = \begin{cases} D_{nn}, & \text{when } n = m, \\ D_{mn}, & \text{when } n \neq m, \end{cases}$$

$$D_{nn} = EI\left(\frac{2n-1}{2L}\right)^4 \times \frac{1}{2}L - EI\left(\frac{2n-1}{2L}\right)^3 \sin\left(\frac{2n-1}{2}\pi\right) + EI\left(\frac{2n-1}{2L}\right)^4 \times \frac{1}{2}L,$$

$$D_{mn} = EI\left(\frac{2n-1}{2L}\right)^3 \sin\left(\frac{2n-1}{2}\pi\right),$$

and

$$P_1 \cdots P_m = P \times L.$$

Similarly, for the Case II boundary conditions

$$EIB_nL\left(\frac{n\pi}{L}\right)^4 = P(1 - (-1)^n), \tag{9}$$

in which $n = 1,\ldots,k$ or in matrix form

$$\begin{bmatrix} D_{11} & 0 & \cdots & 0 \\ 0 & D_{22} & \cdots & 0 \\ \vdots & \cdots & \vdots & \vdots \\ 0 & \cdots & 0 & D_{nn} \end{bmatrix}_{n\times n} \begin{Bmatrix} B_1 \\ \vdots \\ B_{n-1} \\ B_n \end{Bmatrix}_{n\times 1} = \begin{Bmatrix} P_1 \\ \vdots \\ P_{n-1} \\ P_n \end{Bmatrix}_{n\times 1} \tag{10}$$

in which

$$D_{nn} = EIL\left(\frac{n\pi}{L}\right)^4,$$

and

$$P_n = P[1 - (-1)^n].$$

Eqs. (8) and (10), respectively, can also be expressed as the following forms:

$$\mathbf{D} \cdot \mathbf{B} = \mathbf{P} \tag{11}$$

or

$$\mathbf{B} = \mathbf{D}^{-1} \cdot \mathbf{P}. \tag{12}$$

Based on beam theory, once the pile deflection function is determined, the moment $M(z)$, the shear force $V(z)$, and the soil reaction $q(z)$ along the pile shaft can easily be obtained, as given in the following equation:

$$M(z) = EI\frac{\mathrm{d}^2 y(z)}{\mathrm{d}z^2}, \quad V(z) = \frac{\mathrm{d}M}{\mathrm{d}z} \text{ and } q(z) = \frac{\mathrm{d}V}{\mathrm{d}z}. \tag{13}$$

The deflection function given in Eq. (6) is used to fit the deflection data measured using the inclinometer under each applied loading. Hence, an optimised value for k in Eq. (6) and the soil reaction $q(z)$ are needed before $\mathbf{B}$ can be determined from Eqs. (8), (10) and (12). From Eq. (13), it is known that the soil reaction is the fourth differentiation of the deflection function multiplied by the flexural rigidity of the pile. Hence, once the deflection function of the pile–soil system and the flexural rigidity of the pile are known, the soil reaction can be obtained without knowing the soil properties in advance.

To further expand Eq. (6), the computed deflection at depth z can be expressed as

$$\mathbf{Y} = \mathbf{A} \cdot \mathbf{B}, \tag{14}$$

where

$$\mathbf{A}_{j\times n} = \begin{bmatrix} (1 - \cos \bar{N}_n\pi \cdot z_1) & \cdots & (1 - \cos \bar{N}_2\pi \cdot z_1) & (1 - \cos \bar{N}_1\pi \cdot z_1) \\ (1 - \cos \bar{N}_n\pi \cdot z_2) & \cdots & (1 - \cos \bar{N}_2\pi \cdot z_2) & (1 - \cos \bar{N}_1\pi \cdot z_2) \\ \vdots & \vdots & \vdots & \vdots \\ (1 - \cos \bar{N}_n\pi \cdot z_j) & \cdots & (1 - \cos \bar{N}_2\pi \cdot z_j) & (1 - \cos \bar{N}_1\pi \cdot z_j) \end{bmatrix}$$

and

$$\mathbf{B}_{n\times 1} = \begin{Bmatrix} B_n \\ \vdots \\ B_2 \\ B_1 \end{Bmatrix}.$$

The least-square rule is then applied to perform regression to solve $\mathbf{B}_{n\times 1}$ using the procedures described below.

1. Obtain the square summation of the error, $\mathbf{E}$, between the calculated and measured deflections:

$$\mathbf{E} = [\mathbf{A}\cdot\mathbf{B} - \mathbf{Y}]^{\mathrm{T}}[\mathbf{A}\cdot\mathbf{B} - \mathbf{Y}]. \tag{15}$$

2. For minimum error, Eq. (15) has to be satisfied and used to solve $\mathbf{B}_{n\times 1}$ for the optimised values of the coefficients $\{B_n\}$

$$\frac{\partial \mathbf{E}}{\partial \mathbf{B}} = 2\mathbf{A}^{\mathrm{T}}\cdot\mathbf{A}\cdot\mathbf{B} - 2\mathbf{A}^{\mathrm{T}}\cdot\mathbf{Y} = 0. \tag{16}$$

2.3. Regularisation with the Cesaro sum technique

Since the deflection functions of the pile–soil system given in Eq. (6) are Fourier series functions, these functions will cause ill-posed conditions after differentiation. The Cesaro sum technique is used to guarantee the convergence of these Fourier series functions.

The general (C,r) Cesaro sum is defined as [6]

$$S_k = (C,r)\left\{\sum_{n=0}^{k} a_n\right\} \equiv \frac{C_{r-1}^{k+r-1}s_0 + C_{r-1}^{k+r-2}s_1 + \cdots + C_{r-1}^{r}s_{k-1} + C_{r-1}^{r-1}s_k}{C_r^{k+r}}, \tag{17}$$

where $C_r^k = k!/(r!(k-r)!)$, and the partial sum is $s_i = \sum_{n=0}^{k} a_n(z)$.

For computational convenience, the s_i terms are changed to a_i terms, and can be changed to the conventional Cesaro sum

$$S_k = (C,1)\left\{\sum_{n=0}^{k} a_n\right\} \equiv \frac{s_0 + s_1 + \cdots + s_{k-1} + s_k}{k+1}, \tag{18}$$

$$(C,1)\sum_{n=0}^{k} a_n \equiv \frac{1}{k+1}\sum_{n=0}^{k}(k-n+1)a_n. \tag{19}$$

Similarly, the Cesaro sums of $(C,2)$, $(C,3)$ and $(C,4)$ are:

$$S_k = (C,2)\left\{\sum_{n=0}^{k} a_n\right\} \equiv \frac{1}{(k+1)(k+2)} \times \sum_{n=0}^{k}(k-n+1)(k-n+2)a_n, \tag{20}$$

$$S_k = (C,3)\left\{\sum_{n=0}^{k} a_n\right\} \equiv \frac{1}{(k+1)(k+2)(k+3)} \times \sum_{n=0}^{k}(k-n+1)(k-n+2)(k-n+3)a_n, \tag{21}$$

$$S_k = (C,4)\left\{\sum_{n=0}^{k} \alpha_n\right\} \equiv \frac{1}{(k+1)(k+2)(k+4)} \times \sum_{n=0}^{k}(k-n+1)(k-n+2)(k-n+3)(k-n+4)a_n. \tag{22}$$

Or, for the general integer order r, the Cesaro sum can be expressed as

$$S_k = (C,r)\left\{\sum_{n=0}^{k} a_n\right\} = \sum_{n=0}^{k}\frac{(k)!(k+r-n)!}{(k+n)!(k+r)!}a_n. \tag{23}$$

For the case of non-integer order, the Cesaro sum can be expressed as

$$S_k = (C,r)\sum_{n=0}^{k} a_n \equiv \sum_{n=0}^{k} w_n^r a_n, \tag{24}$$

in which the weight is represented by

$$w_n^r = \frac{\Gamma(k+1)\Gamma(k+r+1-n+1)}{\Gamma(k+1-n+1)\Gamma(k+r+1)}, \tag{25}$$

where $\Gamma(x)$ is the Gamma function of x. Eq. (25) reduces to Eq. (23) when r is an integer.

Based on this regularisation technique, the series representations for displacement $y(z)$, slope $\theta(z)$, moment $M(z)$, shear force $V(z)$ and soil reaction $q(z)$ are expressed via the Cesaro sum as:

$$y(Z) = (C,1)\left\{\sum_{n=1}^{k} B_n(1-\cos\bar{N}\pi z)\right\}, \tag{26}$$

$$\theta(z) = y'(z) = (C,2)\left\{\sum_{n=1}^{k} B_n\cdot\bar{N}\cdot(\sin\bar{N}\pi z)\right\}, \tag{27}$$

$$M(z) = EIy''(z) = (C,3)\left\{\sum_{n=1}^{k} EI\cdot B_n\cdot\bar{N}^2\cdot(\cos\bar{N}\pi z)\right\}, \tag{28}$$

$$V(z) = EIy'''(z) = (C,4)\left\{\sum_{n=1}^{k} EI\cdot B_n\cdot\bar{N}^3\cdot(-\sin\bar{N}\pi z)\right\}, \tag{29}$$

$$q(z) = EIy''''(z) = (C,5)\left\{\sum_{n=1}^{k} EI\cdot B_n\cdot\bar{N}^4\cdot(-\cos\bar{N}\pi z)\right\}, \tag{30}$$

in which $\bar{N} = 2n - 1/2L$ and $\bar{N} = n/L$ are for the Case I and Case II boundary conditions, respectively.

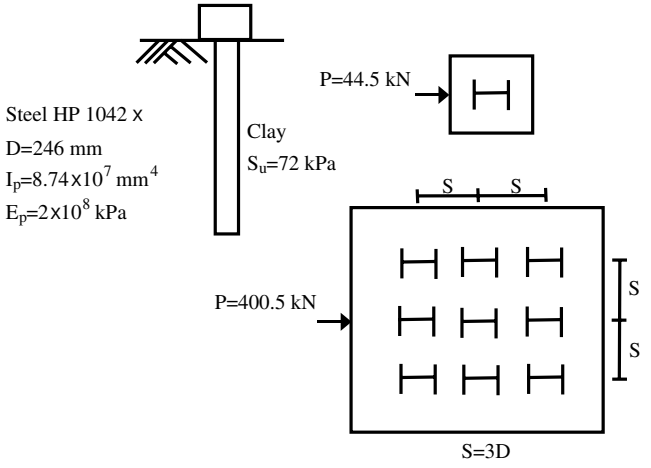

Fig. 3. Arrangement of lateral pile load test of H piles. (Redraw from Focht and Koch [8].)

2.4. Numerical procedures

The procedure involves:

(a) Taking the boundary conditions of the pile and then selecting the pile–soil deflection function from Eq. (6).
(b) Substituting inclinometer measurement data into Eq. (14) and then determining **B** from Eq. (16).
(c) Using the deflection function obtained from procedure (b) and utilising the Cesaro sum technique in Eqs. (28)–(30) to obtain the moment, shear and soil reaction along the pile shaft.
(d) Using Eqs. (26) and (30) to obtain the $p-y$ curves.

For pile groups, the deflection of all piles needs to be monitored separately. Hence, individual piles in a group are analysed separately.

3. Examples

The use of the technique described above is illustrated using three field lateral loading 13 tests, one H pile case and two pipe pile cases, and comparisons are made with the results obtained using other methods.

3.1. Lateral pile–load test of H piles

Focht and Koch [8] reported lateral load tests for both single and group steel H piles. Fig. 3 shows the schematic layout of the tests. The piles had a width $D = 246$ mm, moment of inertia $I_p = 8.74 \times 10^7$ mm^4, and elastic modulus $E_p = 2 \times 10^8$ kPa. The piles, joined by a cap, were first driven into a medium-stiff clay

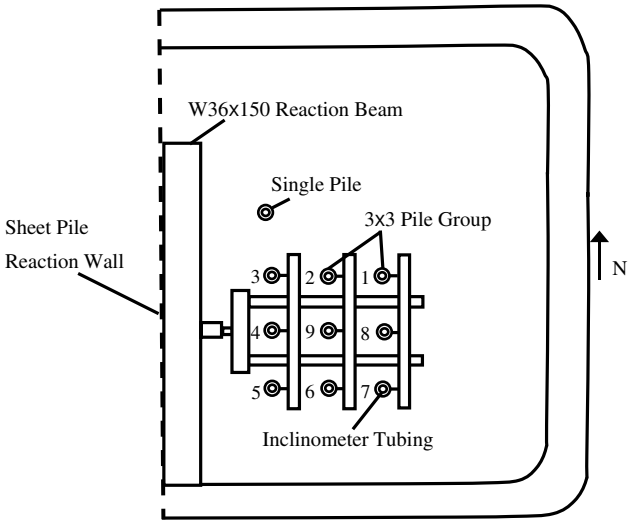

Fig. 5. Arrangement of 3 by 3 pipe pile tests (without cap). (Redraw from Rollins et al. [10].)

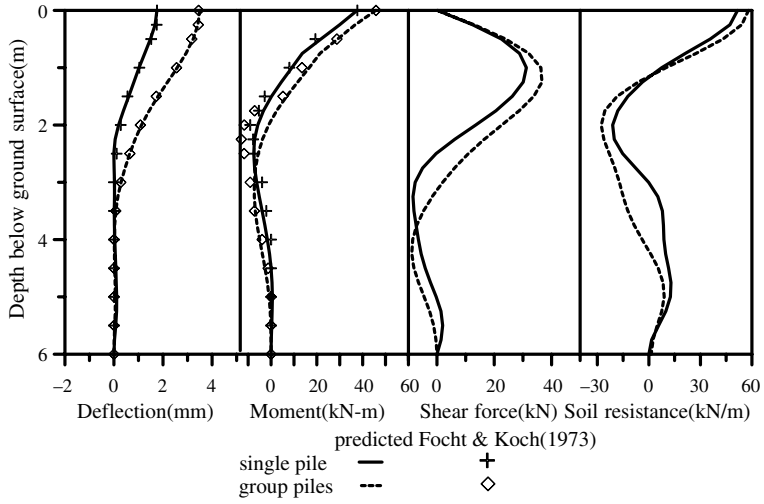

Fig. 4. The deflection, slope, bending moment, shear force, and soil resistance distributions along the pile shaft of H piles.

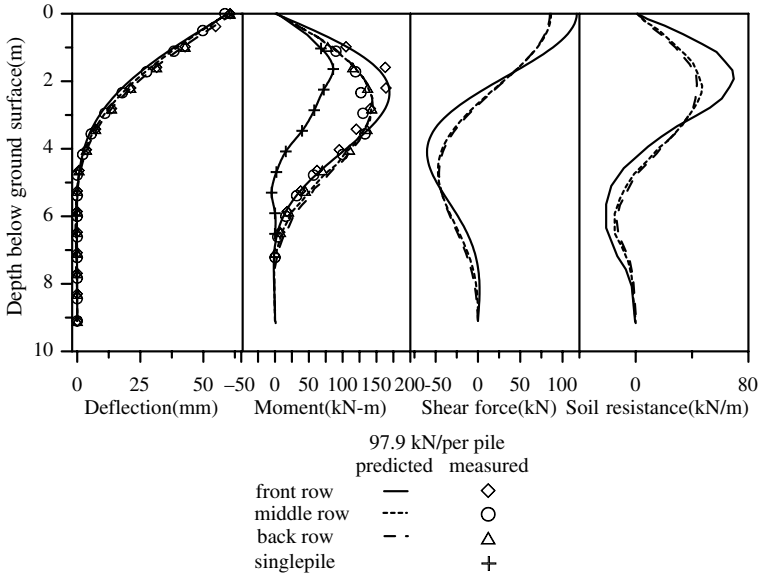

Fig. 6. Deflection, slope, bending moment, shear force, and soil resistance distributions along the pile shaft of piles group under lateral load of 97.9 kN/per pile.

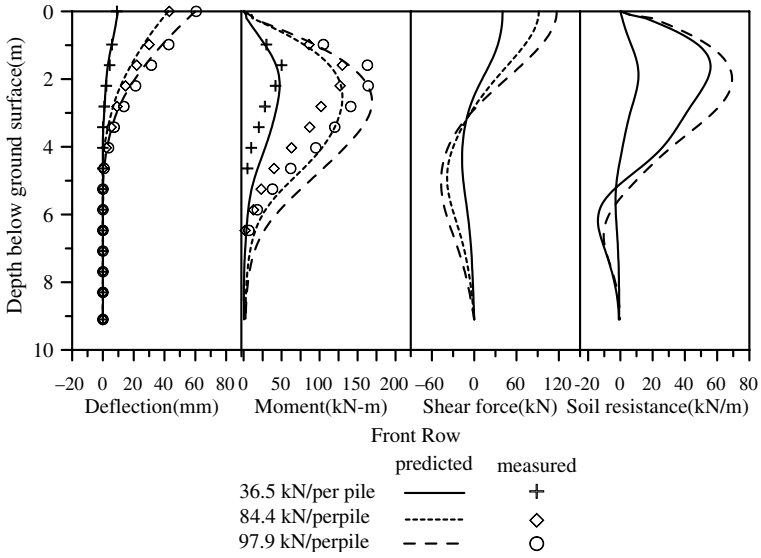

Fig. 7. Deflection, slope, bending moment, shear force, and soil resistance distributions along the pile shaft of front row piles (without cap).

deposit with undrained shear strength of 72 kPa. The Case II boundary condition was considered in the analysis for both the single pile and the pile group. Calculated and measured deflections and bending moment distributions of the single pile and pile group subjected to lateral loads of 44.5 kN per pile are shown in Fig. 4. As shown, the proposed method was able to successfully reproduce the deflections and bending moment distribution in reasonable agreement with the measurements. The maximum moment of the pile group is 1.2-fold higher than that of the single pile. The deflection of any pile in a group causes movement of the surrounding soil and piles, thus leading to greater deflection for the pile group than for single piles subjected to the same load per pile [9]. The maximum bending moment in the group is greater than that for the single pile, because the soil allows the group to deflect more for the same load per pile, and the soil thus behaves as if it is softer [9].

3.2. Pipe pile tests

A full-scale laterally loaded pile group was tested at Salt Lake International Airport, Utah, USA by Rollins

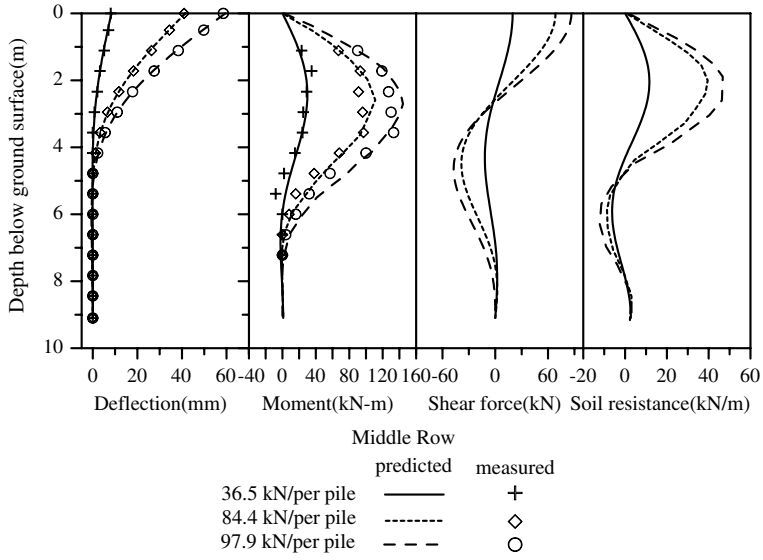

Fig. 8. Deflection, slope, bending moment, shear force, and soil resistance distributions along the pile shaft of middle row piles (without cap).

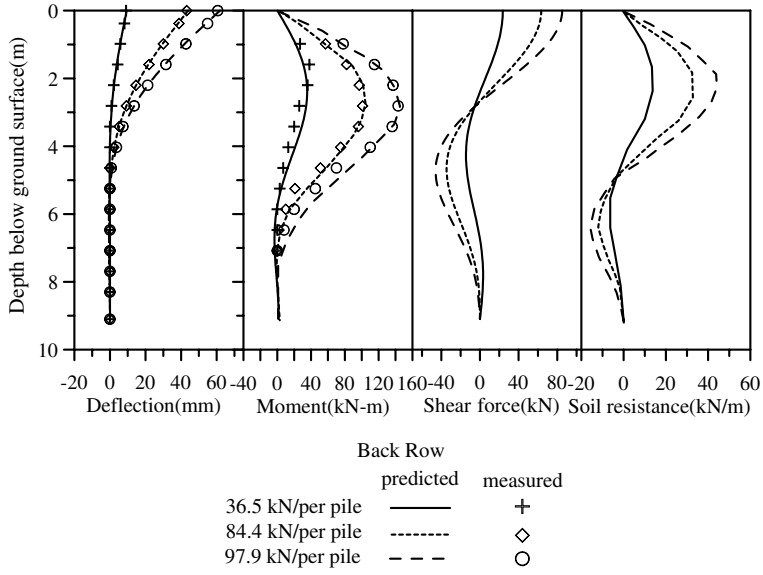

Fig. 9. Deflection, slope, bending moment, shear force, and soil resistance distributions along the pile shaft of back row piles (without cap).

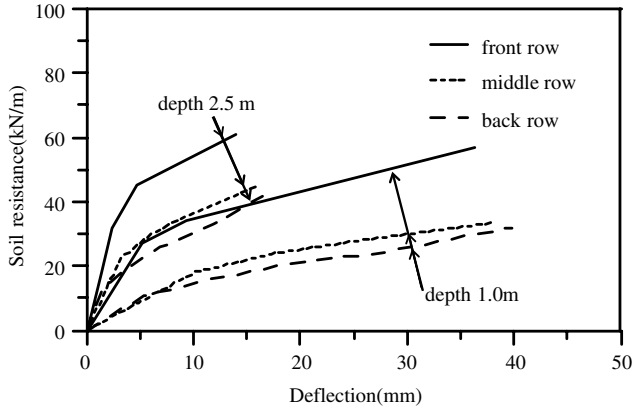

Fig. 10. *p–y* curves of group piles without cap.

et al. [10]. The pile groups were driven in a 3×3 pattern with a nominal spacing of three pile diameters centre-to-centre into a soil profile consisting of 14 soft to

Table 1
Summary of the suggested *p*-multipliers of 3 by 3 pipe pile group tests

Pile row	*p*-Multipliers from this study		*p*-Multipliers (Rollins et al. [10]; Rollins and Sparks [13])	
	Without cap	With cap	Without cap	With cap
Front	0.58	0.66	0.63	0.60
Middle	0.42	0.54	0.38	0.40
Back	0.40	0.52	0.43	0.40

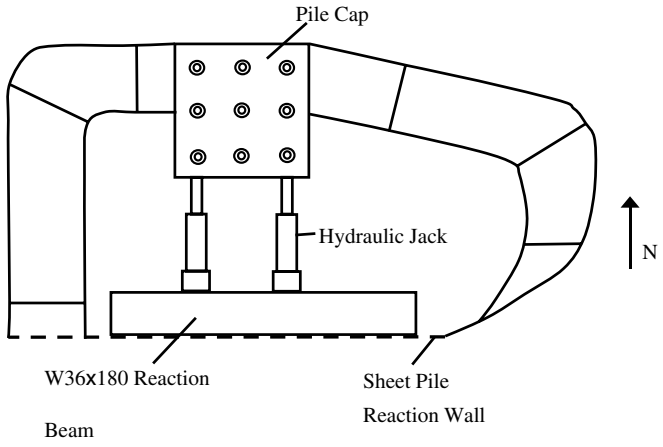

Fig. 11. Arrangement of 3 by 3 pipe pile tests with cap. (Redraw from Rollins and Sparks [13].)

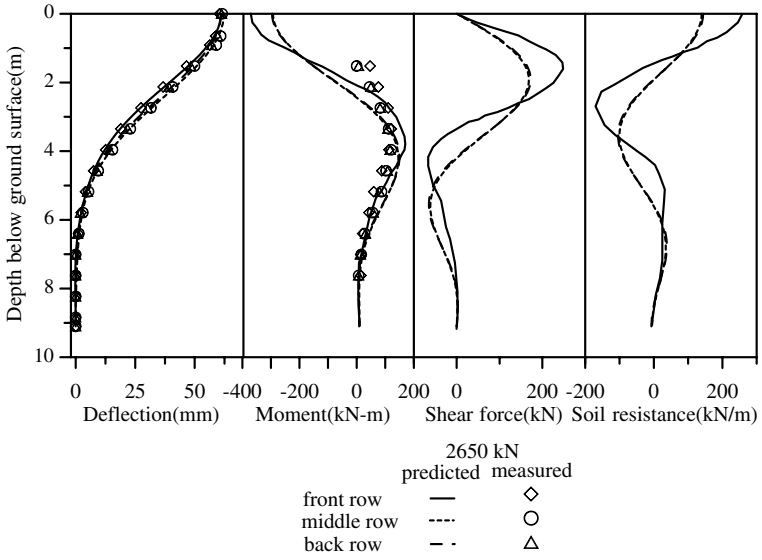

Fig. 12. Deflection, slope, bending moment, shear force, and soil resistance distributions along the pile shaft of piles group under lateral load of 2650 kN.

medium-stiff clays and silts underlain by sand. Closed-ended steel pipe piles with a 9.5-mm wall thickness and 0.305-mm inner diameter were driven approximately 9.1 m below the ground surface. The elastic modulus and minimum yield stress of the steel were 200 GPa and 331 MPa, respectively. The pipe piles were infilled with concrete with a compressive strength and elastic modulus of 20.7 MPa and 17.5 GPa, respectively. The layout of the test is shown in Fig. 5, in which the number next to each pile is the pile driving order. Since concrete was infilled into the pipe piles, the moment of inertia for the concrete was computed using ACI-318-95 [11] to account for cracking. Hence, the moment of inertia of the piles was updated for each load increment. Assuming Case I boundary conditions for the free-headed pile cases, the results calculated for the pile group due to an average load of 97.9 kN/per pile and for a single pile subjected to the same loading are given in Fig. 6. Both calculated and measured results show that the front row has the highest maximum moment, occurring 2.3 m below the ground surface, which is approximately 23% higher than that of the middle and back rows. Fig. 6 also gives the magnitude of the moments that occur at each row of piles, with the front row > back row > middle row > a single pile. The deflection, moment, shear force and soil resistance along the pile shaft of each row due to the different loading levels are given in Figs. 7–9 for comparison. The $p-y$ curves obtained at several different depths for each row of piles are given in Fig. 10, in which the front-row piles carry significantly higher soil resistance than the middle and back rows of piles. The

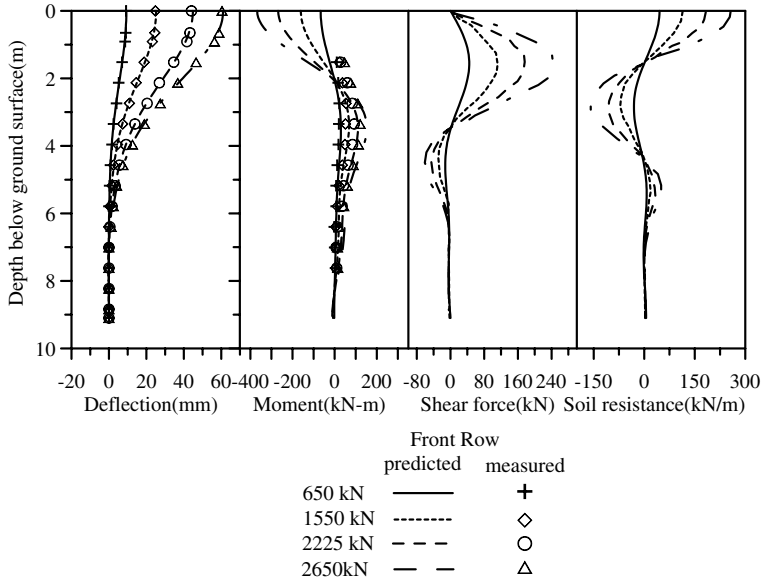

Fig. 13. Deflection, slope, bending moment, shear force, and soil resistance distributions along the pile shaft of front row piles with cap.

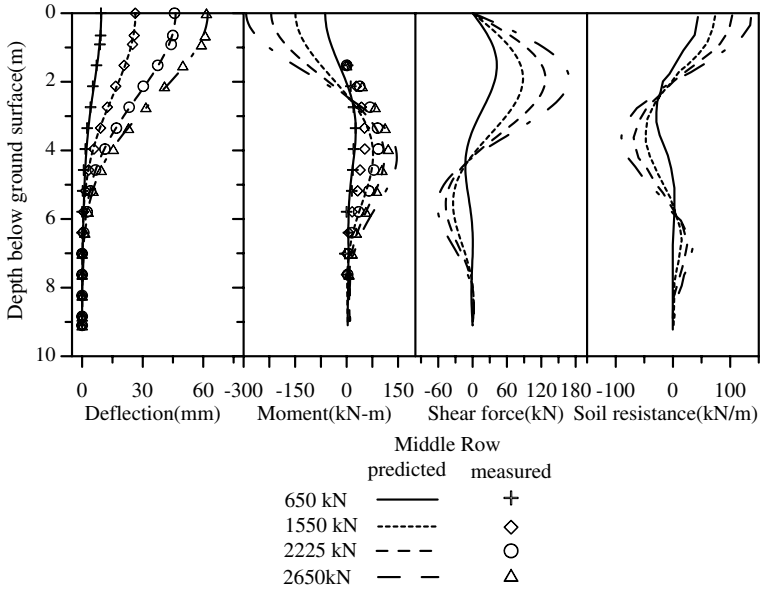

Fig. 14. Deflection, slope, bending moment, shear force, and soil resistance distributions along the pile shaft of middle row piles with cap.

p-multiplier for this pile group without a cap is suggested in Table 1, in which the results back-calculated from LPILE [12] by Rollins et al. [10] are also given for comparison.

The pile group shown in Fig. 5 was subjected to lateral load testing again by Rollins and Sparks in 2002 [13]; however, the pile group was constrained by a 2.74 m × 2.74 m cap on the top of the pile group (Fig. 11). Hence, the Case II boundary condition was considered for analysis due to the constraint from the cap. The analytical results are given in Fig. 12. Because of the constraint of the pile cap, the front-row piles still show the largest moment, and the moments in the middle and back rows have almost the same values. Again, the deflection, moment, shear force and soil resistance along the pile shaft due to the different loading levels for different rows are given in Figs. 13–15 for the purposes of comparison. Derived $p-y$ curves are shown in Fig. 16, in which the soil resistance of the front-row piles is 58% higher than that of the middle and back rows of piles. Again, the *p*-multiplier for the capped pile group is also given in Table 1 for comparison with the *p*-multipliers suggested by Rollins and Sparks [13].

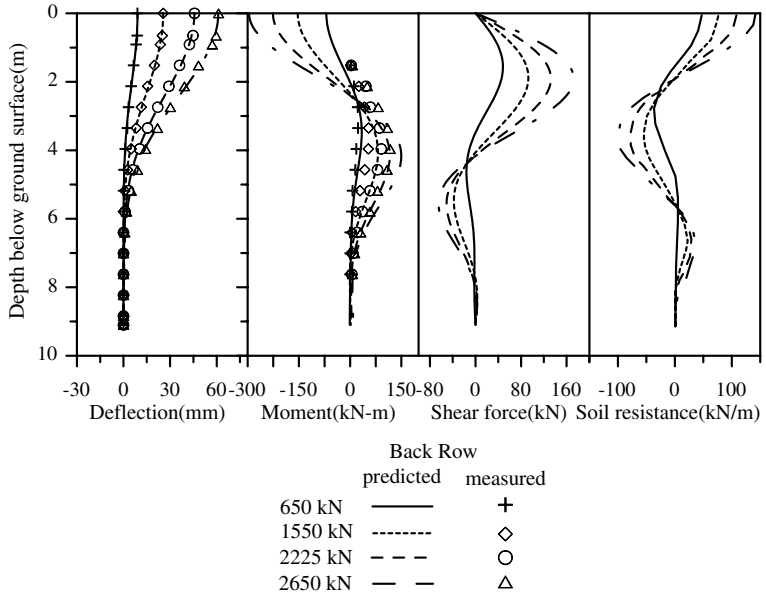

Fig. 15. Deflection, slope, bending moment, shear force, and soil resistance distributions along the pile shaft of back row piles with cap.

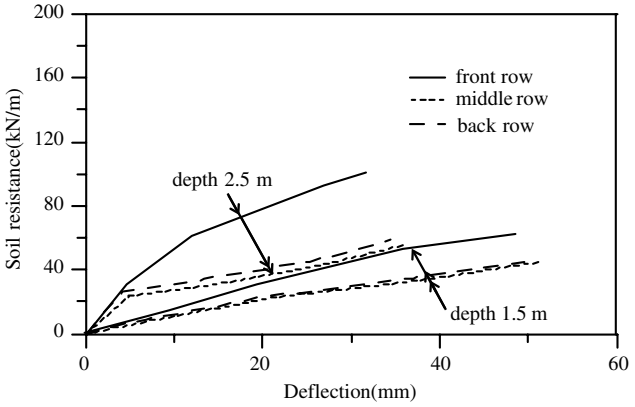

Fig. 16. p–y curves of group piles with cap.

4. Summary and conclusions

In this paper, a simple method for interpreting laterally loaded pile test results is proposed. The theoretical background and a detailed derivation of the proposed analytical method are described. The feasibility of the method developed was verified using the results of three pile-test case histories. The advantages of the proposed analytical method include: (1) in addition to satisfying boundary conditions for pile heads either free or fixed with sway, the deflection function derived can be used to describe lateral load behaviour of a single pile or a pile group system and (2) only inclinometer data are needed to derive the deflection function.

It should be pointed out that for short piles with high lateral loading, permanent lateral displacement might occur at the bottom of the piles. The definitions of strain energy and potential energy used in this study need to be modified to establish the energy conservation relation. Furthermore, energy conservation of the soil–pile system cannot be included using only inclinometer data. Further study is needed to develop the analytical model for short pile applications.

References

[1] Pinto PL, Anderson B, Townsend FC. Comparison of horizontal load transfer curves for laterally loaded piles form strain gages and slope inclinometer: a case study. In: Field instrumentation for soil and rock, ASTM STP 1358, 1999; 3–15.

[2] Brown DA, Hidden SA, Zhang S. Determination of p–y curves using inclinometer data. Geotech Test J 1994;17(2):150–8.

[3] Wang ST, Reese LC. Analysis of piles under lateral load – computer program COM624P for the microcomputers. Report No. FHWA-SA-91-002, US Department of Transportation, FHWA, Washington, DC, USA; 1991.

[4] Chen JT, Hong HK, Yeh CS, Chyuan SW. Integral representations and regularizations for a divergent series solution of a beam subjected to support motions. Earthquake Eng Struct Dyn 1996;25:909–25.

[5] Wang JTS, Lin CC. A method for exact series solutions in structural mechanics. J Appl Mech 1999;66:380–7.

[6] Hardy GH. Divergent series. London: Oxford University Press; 1949.

[7] Wunderlich W, Pilkey WD. Mechanics of structures: variational and computational methods. Boca Raton (FL): CRC Press; 2003.

[8] Focht JA, Koch KJ. Rational analysis of the lateral performance of offshore pile groups. In: Proceeding of the 5th offshore technology conference 1973, Dallas, Texas, 1997; 701–8.

[9] Ooi PSK, Duncan JM. Lateral load analysis of groups of piles and drilled shafts. J Geotech Eng ASCE 1994;120(6): 1034–50.

[10] Rollins KM, Peterson KT, Weaver TJ. Lateral load behavior of full-scale pile group in clay. J Geotech Geoenviron Eng ASCE 1998;124(6):468–78.

[11] American Concrete Institute. ACI building code requirements for structural 18 concrete and commentary. ACI 318-95, Farmington Hills, Michigan, USA; 1995.

[12] Reese LC, Wang ST. Documentation of computer program LPILE version 4.0 for windows. Austin, TX, USA: Ensoft, Inc.; 1994.

[13] Rollins KM, Sparks A. Lateral resistance of full-scale pile cap with gravel backfill. J Geotech Geoenviron Eng ASCE 2002;128(9):711–23.